JOURNAL OF SPACECRAFT AND ROCKETS
Vol. 45, No. 6, November–December 2008

Effect of Freestream Noise on Roughness-Induced Transition for the X-51A Forebody

Matthew P. Borg* and Steven P. Schneider†
Purdue University, West Lafayette, Indiana 47097-1282

DOI: 10.2514/1.38005

A 20%-scale X-51A forebody model was tested in the Boeing and U.S. Air Force Office of Scientific Research Mach-6 Quiet Tunnel. The effect of a smooth blank and two different trip strips on windward-forebody transition was measured using temperature-sensitive paint and hot-wire anemometry. Reducing freestream noise from conventional to quiet levels increased the smooth-wall transition Reynolds number by a factor of at least 2.2. In addition, the transition Reynolds number based on the distance from the trips increased by a factor of 2.4 for the smaller trips and by a factor of 1.7 for the larger trips. Thus, tunnel noise had a substantial effect on roughness-induced transition.

Introduction

LAMINAR-TURBULENT transition in hypersonic boundary layers is important for prediction and control of heat transfer, skin friction, and other boundary layer properties. Vehicles that spend extended periods at hypersonic speeds may be critically affected by the uncertainties in transition prediction, depending on their Reynolds numbers. However, the mechanisms leading to transition are still poorly understood, even in low-noise environments.

Many transition experiments have been carried out in conventional ground-testing facilities over the past 50 years [1]. However, these experiments are contaminated by the high levels of noise that radiate from the turbulent boundary layers normally present on the wind tunnel walls [2]. These noise levels, typically 0.5–1% of the mean, are an order of magnitude larger than those observed in flight [3,4]. These high noise levels can cause transition to occur an order of magnitude earlier than in flight [2,4]. In addition, the mechanisms of transition operational in small-disturbance environments can be changed or bypassed altogether in high-noise environments; these changes in the mechanisms change the parametric trends in transition [3]. Mechanism-based prediction methods must be developed, supported in part with measurements of the mechanisms in quiet wind tunnels.

For supersonic and hypersonic speeds, there have been only a few experiments that explore the effects of tunnel noise on roughness-induced transition [3]. Creel et al. [5] performed experiments on swept circular cylinders at Mach 3.5 under low freestream noise levels and also nearly conventional levels. For the smooth-walled case, changing the tunnel noise levels was found to have no effect on transition. When small trips were added to the model, the transition Reynolds number was found to increase when the tunnel noise levels were decreased. Ito et al. [6] performed an experimental study on a model of an axisymmetric scramjet forebody at Mach 4 for a Reynolds number of $4.5 \times 10^6/\text{m}$ $(1.4 \times 10^6/\text{ft})$. The model included two compression corners. Data were collected with different-sized boundary-layer trips placed near the model nosetip under low freestream noise levels and also freestream noise levels approximately 6-times higher. All the trip sizes were thought to be much larger than the boundary-layer thickness and, thus, significantly larger than realistic trips. Ito et al. found that reducing the tunnel noise levels dramatically decreased intermittency and so delayed transition significantly.

Purdue University is examining boundary-layer stability and transition on the X-51A forebody. The X-51A is a waverider-type scramjet-powered hypersonic vehicle with a hydrocarbon fuel. The Purdue model is 20% scale for the portion of the vehicle forward of the engine inlet. Experiments using temperature-sensitive paint (TSP) and hot-wire anemometry were conducted to characterize the effect of tunnel noise on transition. These experiments were conducted on the windward side in the Boeing and U.S. Air Force Office of Scientific Research Mach-6 Quiet Tunnel (BAM6QT).

For the X-51A to operate as intended, the boundary layer entering the engine must be turbulent. This reduces the risk of unstart due to shock-wave interactions with the boundary layer in the isolator and also allows more rapid mixing and burning within the combustor. To ensure a turbulent boundary layer, boundary-layer trips must be added to the vehicle geometry upstream of the engine inlet. If the trips are too small, the boundary layer may remain laminar into the engine and prevent it from starting. If the trips are oversized, they will add unnecessary drag to the vehicle. Oversized trips may also reduce engine performance.

Such trips must be designed using empirical measurements. However, most hypersonic wind tunnels have turbulent-wall boundary layers that radiate a good deal of acoustic noise into the flow. It is reasonable to expect that this high-noise environment could change the effectiveness of trips on the model and induce early roughness-dominated transition. If the flight trips were designed based on ground tests in conventional facilities with high noise, it is possible that they would be undersized and fail to trip the boundary layer in the low-noise flight environment. This could lead to significantly reduced performance or even loss of the vehicle.

Given the uncertainty of the effect of freestream noise on roughness-dominated transition, the effect of tunnel noise on tripping should be evaluated in a low-noise environment. Thus, the current experiments determine the effect of conventional and quiet noise levels on three different configurations of the X-51A forebody-roughness in the BAM6QT.

Development of Quiet-Flow Wind Tunnels

Only in the last two decades have low-noise supersonic wind tunnels been developed [2,7]. This development has been difficult because the test-section wall boundary layers must be kept laminar in order to avoid high levels of eddy-Mach-wave acoustic radiation from the normally-present turbulent boundary layers. A Mach 3.5 tunnel was the first to be successfully developed at NASA Langley

Presented as Paper 592 at the 46th AIAA Aerospace Sciences Meeting and Exhibit, Reno, NV, 7–10 January 2008; received 10 April 2008; revision received 26 August 2008; accepted for publication 28 August 2008.

*Graduate Research Assistant, School of Aeronautics and Astronautics. Student Member AIAA.

†Professor, School of Aeronautics and Astronautics. Associate Fellow AIAA.

Research Center [8]. NASA also operated a prototype quiet Mach 6 facility through 1995. It was removed from service due to operational conflicts and changing research priorities. The facility is now housed at Texas A&M University. The Langley Mach 6 tunnel was used as a starting point for the Purdue nozzle [9]. The Purdue Mach 6 tunnel is presently the only operational hypersonic quiet tunnel anywhere in the world [10].

Boeing/U.S. Air Force Office of Scientific Research Mach 6 Quiet Tunnel

Quiet facilities require low levels of noise in the inviscid flow entering the nozzle through the throat and laminar boundary layers on the nozzle walls. To reach these low noise levels, conventional blow-down facilities must be extensively modified. Requirements include a 1 μm particle filter, a highly polished nozzle with bleed slots for the contraction-wall boundary layer, and a large settling chamber with screens and sintered-mesh plates for noise reduction [2]. To reach these low noise levels in an affordable way, the Purdue facility has been designed as a Ludwieg tube [10]. A Ludwieg tube is a long pipe with a converging–diverging nozzle on the end, from which flow exits into the nozzle, test section, and second throat. Care is taken to keep the air in the tunnel as dry as possible to avoid water condensation in the nozzle. The dew point of the air in the tunnel, measured with a capacitance-type dew point meter, is typically on the order of -20°C (-4°F).

A pair of diaphragms is placed downstream of the test section. When the diaphragms burst, an expansion wave travels upstream through the test section into the driver tube. Because the flow remains quiet after the wave reflects from the contraction, sufficient vacuum can extend the useful runtime to many cycles of expansion-wave reflection, during which the pressure drops quasi-statically.

The contraction-wall boundary layer is bled off just upstream of the throat, beginning a fresh, undisturbed boundary layer for the nozzle wall. The bleed air is reintroduced to the main flow in the diffuser, far downstream of the throat.

When operated quietly, the nozzle-wall boundary layer in the BAM6QT remains laminar, producing freestream noise levels on the order of 0.05%. When operated conventionally, the nozzle-wall boundary layer is turbulent and the noise level increases to about 2–3%. This is higher than the noise levels in many conventional facilities, in part due to the small cross section of the BAM6QT. However, much remains uncertain regarding the noise levels in other facilities with turbulent-wall boundary layers. Lafferty et al. [11] report noise levels between 2 and 3.5% at Mach 8 and 3.75 to 6.25% at Mach 14 . Schneider [3] reports high mass-flow fluctuations for several other hypersonic facilities.

Experiments on the X-51A Forebody

The experiments reported here were all on the windward side of the model at an inviscid Mach number of 6.0 with an initial stagnation temperature of $T_0 = 433$ K (780°R) at 4.0 deg angle of attack. The Purdue model is 20% scale and includes the forebody up to the engine inlet cowl. A drawing of the full flight vehicle is shown in Fig. 1. The portion that corresponds to the current model is circled.

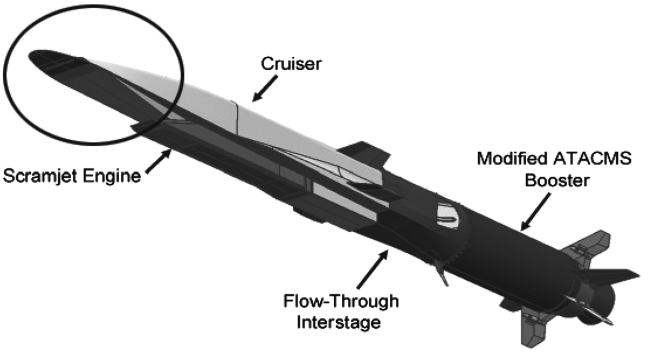

Fig. 1 Full X-51A vehicle (from [21]) with the portion corresponding to the model circled.

The model consists of a stainless steel nose section with an aluminum afterbody, as shown in Fig. 2. The model includes a nylon 6/6 insert on both the windward and leeward sides. The nylon inserts were included to act as a thermal insulator layer for TSP. Liu and Sullivan [12] present a good background of the physics of TSP. Matsumura et al. [13] successfully employed the TSP technique on a generic scramjet forebody in the BAM6QT. The methodology used in the present experiments is very similar to his.

For the purposes of the present experiments, TSP is fairly quantitative in temperature. Efforts are underway to make it reliably quantitative in temperature and heat transfer. At present, the uncertainties associated with this method are too large for accurate quantitative results. However, this technique has demonstrated consistently that temperature scales monotonically with intensity. To reliably measure the location of transition, precise temperatures are not needed.

There are several uncertainties regarding this technique and its use in the BAM6QT. The effect of pressure on the luminescence of the paint is unknown. Matsumura et al. [14] did a preliminary investigation of this uncertainty. Additionally, the current calibration instrumentation only measures temperature to a precision of 1 K (2°R). This introduces uncertainty into the calibration. The effect of nonuniformities in the thickness of the paint layer is also unknown. Finally, the effect of variations in the initial model-substrate temperature has not been thoroughly investigated.

The assembled model is 34.42 cm (13.55 in.) long. The windward nylon insert is approximately 23.9 cm (9.4 in.) long and 3.0 cm (1.2 in.) wide. The insert is composed of a 1.02-cm (0.4-in.)-long flat surface followed by a compression corner. The remainder of the insert maintains a constant angle to the flow and a constant width. The nylon is coated with Ru(bpy) luminophore molecules in DuPont ChromaClear® paint. It was calibrated to give surface temperatures. A photograph of the windward surface of the model is seen in Fig. 2. For all of the data, the entire nylon insert was imaged. Flow is from left to right.

A Photometrics SenSysB scientific-grade charge-coupled device (CCD) camera was used to obtain all TSP images. Light at 464 nm was used to excite the paint. During each run, photographs were taken as fast as the hardware would allow, about one image every 0.6 s. When the oscilloscopes trigger at tunnel startup, the camera

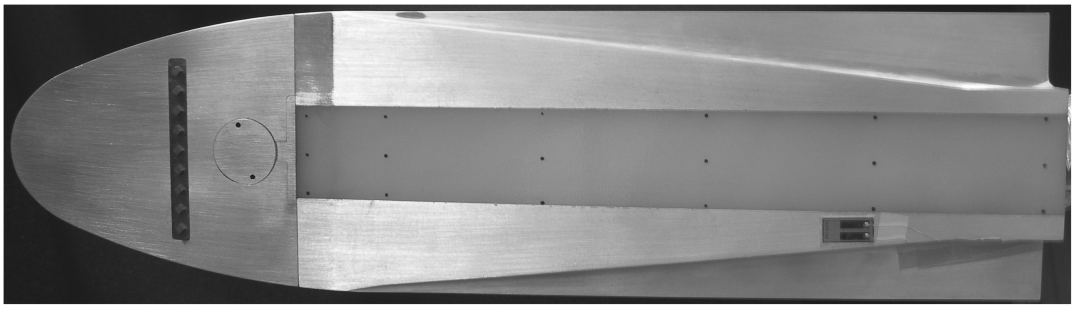

Fig. 2 Photograph of windward side of model.

begins taking pictures with a manually set exposure length. The exposure was generally set to less than 200 ms. The camera outputs a signal when the shutter is open. This signal was recorded and used in subsequent data processing to calculate Reynolds numbers for each image. The x coordinates reported are not arc length, as the outer mold line data of the model have not been provided. Rather, they are a projection of the axial arc length onto a plane at 0 deg angle of attack above the model surface. Given the slight inclination of the model surface, using this definition of x is not much different than using actual arc length. The y coordinates reported in some figures correspond to spanwise location, with $y = 0$ being the centerline.

A smooth strip and two trip strips with different roughnesses were used in the model at a streamwise location of $x = 6.30$ cm (2.48 in.). One of the trip strips is composed of ramp-shaped roughness elements whereas the other has diamond-shaped trips. The roughnesses have the same shape as those used by Berry et al. [15] on the Hyper-X model. Berry's trips were designed to generate a series of counter-rotating vortex pairs that were somewhat smaller than the boundary-layer height. The diamond-shaped trips had been found to be successful for experiments at NASA Langley involving the Space Shuttle Orbiter, X-38, NASP, Hyflite, and HySTP programs [15].

A photograph of the three strips used in the Purdue model can be seen in Fig. 3. Here, the flow is from top to bottom. The upstream edge of the ramp roughnesses are at the same height as the model surface. Moving downstream, they rise up above the model surface and also become increasingly narrow. At the downstream edge, the ramps have a maximum height of 0.076 cm (0.030 in.). Because of difficulties in getting the strip to fit in the model, a 0.013 cm (0.005 in.) shim was placed under the insert. This caused small forward-facing steps at both the upstream and downstream edges of the strip. A skilled machinist measured the step heights along the centerline and found them to be about 0.013 cm (0.005 in.) for the upstream step and 0.008 cm (0.003 in.) for the downstream step. The diamond roughness strip has diamond-shaped roughness elements that are 0.305 cm (0.120 in.) wide across the diagonal and 0.152 cm (0.060 in.) high. The diamond strip was flush with the model surface. For the ramp strip, the model centerline runs between two roughness elements. For the diamond case, the centerline runs directly through a roughness element.

Effect of Tunnel Noise

Runs were made with an initial stagnation pressure of 655 kPa (95 psia) with all three inserts in the model. The tunnel was run under noisy and quiet conditions to assess the effects of noise on natural and roughness-influenced transition.

When the tunnel is run noisy (with the throat bleed suction turned off), the total mass flux out of the driver tube decreases by about 28% from the bleeds-open case, the nozzle-wall boundary layer becomes turbulent, the flow becomes noisy, and the mean Mach number decreases from about 6.0 to about 5.8 due to the difference in the displacement thicknesses between the laminar and turbulent boundary layers. This, in turn, means that the freestream Reynolds number drop with time is less with the bleeds closed than with the bleeds open. When comparing data taken under noisy and quiet conditions, a choice needed to be made regarding whether to compare data at the same freestream Reynolds number or to compare data taken at the same time after the start of the run. The problem with comparing data at the same Reynolds number is that these data were taken at significantly different times during the run. It has been observed that over the course of a run, the mean temperature of the nylon increases.

This effect can be clearly seen in Fig. 4. Shown here are streamwise temperatures for two different runs with low noise, initial stagnation pressures of 804 and 939 kPa (116.6 and 136.2 psia), and equal initial stagnation temperatures of 433 K (779°R). The runs will be referred to as run a and run b, respectively. The gaps in the data are due to the registration marks along the model centerline. The dashed line denotes the location of the compression corner. These data were

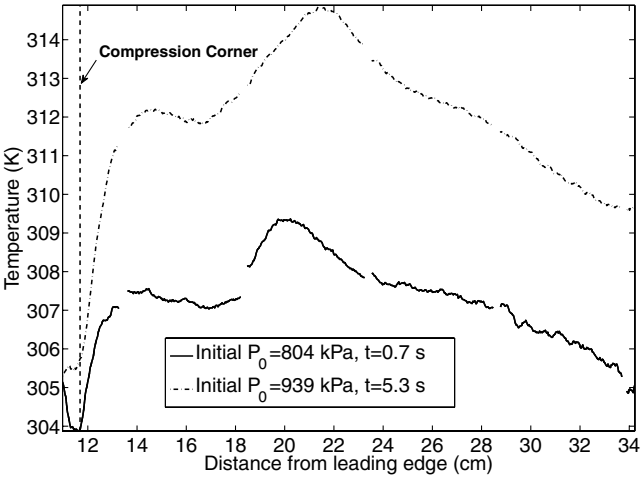

Fig. 4 Centerline temperature for two runs at $Re = 8.5 \times 10^6$/m (2.6×10^6/ft) but at different times into the runs due to different initial conditions.

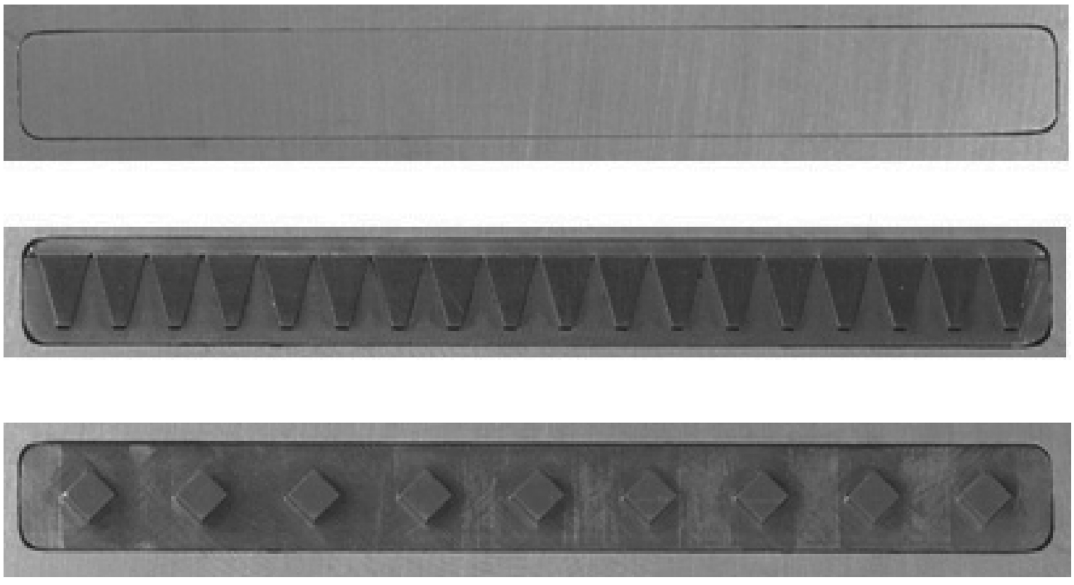

Fig. 3 Trip inserts for model.

collected when the freestream Reynolds numbers were 8.5×10^6/m (2.6×10^6/ft). This condition was met at $t = 0.7$ s for run a and $t = 5.3$ s for run b. For run a, the stagnation pressure had decreased 2.4% and the stagnation temperature had decreased by 1.4%. For run b, these values were 28.2 and 9.4%, respectively. Even though the freestream Reynolds numbers are matched for these streamwise plots, the mean temperature of run b at $t = 5.3$ s is 4.7 K (8.3°R) higher than the mean temperature of run a at $t = 0.7$ s. This is a significant difference considering that the maximum temperature change along the centerline for the data from run a is only 5.5 K (9.9°R). Additionally, the streamwise location of the highest temperature does not match for the two cases; for run b, it is 1.4 cm (0.6 in.) downstream of the peak shown for run a.

Thus, images taken at different times during the run are not readily compared in terms of temperature or heat transfer. It was therefore decided to compare data taken at similar times into a run. This leads to a small variation in Reynolds numbers when comparing these data. The difference in the Mach number between quiet and noisy tunnel runs also leads to a difference in Reynolds number, even if stagnation conditions are the same.

In addition to the TSP data, an uncalibrated polyimide-substrate hot film was glued on 26.7 cm (10.5 in.) downstream of the leading edge and about 3.18 cm (1.25 in.) off the centerline, as shown in Fig. 2. The manufacturer-supplied temperature coefficient was 0.34%°C. It was always operated with an in-house constant temperature anemometer (CTA) at an overheat ratio of 1.31, based on resistances, giving the film a temperature of 389 K (700°R). This hot film was used to determine if the boundary layer was laminar or turbulent. Schmisseur et al. [16] used a similar technique in Purdue's Mach 4 Quiet Tunnel. The data were recorded on a Textronix DPO7054 oscilloscope at a sampling rate of 2×10^6 samples per second. The oscilloscope was operated in Hi-Res mode whereby the 8-bit data were sampled at a higher frequency and then averaged on the fly into memory to obtain 11–12 bits at the set sampling frequency.

TSP and hot-film data will first be presented for the smooth-insert case. TSP and hot-film data will then be shown for both the ramp and diamond trips. At present, the TSP technique is not able to provide reliable quantitative heat-transfer rates. To verify what was suspected from the TSP data, a hot-wire boundary-layer probe was used to determine the state of the windward boundary layer at different streamwise locations for the quiet runs with trip strips. The hot-wire data will be shown for a slightly lower freestream Reynolds number. When the hot-wire data were collected, the maximum quiet pressure in the BAM6QT had dropped from 655 kPa (95 psia) to around 552 kPa (80 psia). This meant that hot wires could not be used at the same conditions as those in the previous measurements. It was thought that the 11% drop in initial Reynolds number would not make much difference in the results. Nevertheless, for completeness, new TSP images at the reduced quiet-flow conditions were obtained for the ramp and diamond roughness inserts. Additionally, at this reduced pressure, the nozzle-wall boundary layer tended to separate for about 1 s some time between 1.0 and 1.5 s into the run. Thus, images shown for the reduced quiet pressure runs were always the second image captured, instead of the fourth as for the higher-pressure runs. This was generally about 0.6 s into the run.

Smooth Insert

Figure 5 shows the surface temperature distributions with the smooth insert under quiet and noisy conditions, at freestream Reynolds numbers of 6.59 and 7.38×10^6/m (2.01 and 2.25×10^6/ft), respectively. The freestream Reynolds numbers are calculated using an isentropic theory for Ludweig tubes [17]. This theory takes into account the falling stagnation pressure and temperature inherent in a blow-down facility. The stagnation temperatures (T_0) and pressures (P_0) were $T_0 = 418$ K (752°R) and $P_0 = 586$ kPa (85 psia) with the tunnel running quietly. With the noisy tunnel, $T_0 = 424$ K (763°R) and $P_0 = 621$ kPa (90 psia). The dashed red line indicates the compression corner. Figure 6 shows the streamwise temperature distribution on the centerline. The gaps in the data are again due to the registration marks on the model surface. The compression corner is marked by the dashed black line.

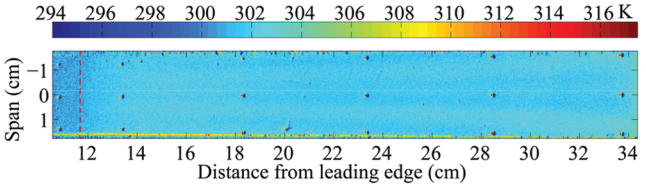

a) Surface temperature for quiet flow, smooth insert, *Re*=6.59x10⁶/m (2.01x10⁶/ft)

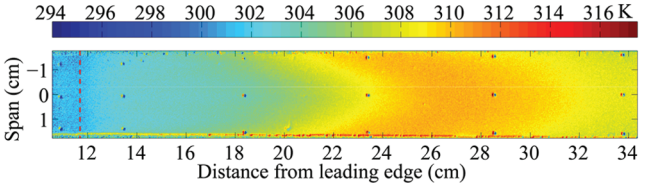

b) Surface temperature for noisy flow, smooth insert, *Re*=7.38x10⁶/m (2.25x10⁶/ft)

Fig. 5 Surface temperature (K) under quiet and noisy conditions with smooth trip insert.

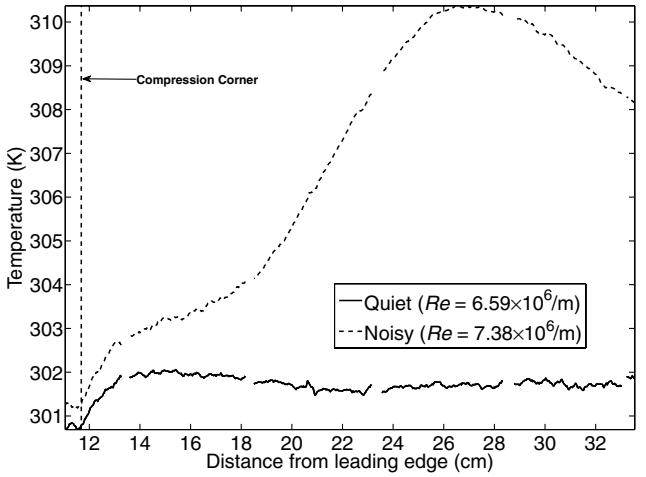

Fig. 6 Centerline temperature for smooth-insert for quiet and noisy flow.

Under quiet conditions, both the TSP image and the centerline temperature distribution show that the temperature increases downstream of the compression corner followed by a nearly monotonic decrease for the rest of the extent of image. This strongly suggests a laminar boundary layer over the entire length of the nylon insert. Faint streaks are also visible in the TSP image. They are most likely due to the presence of streamwise vortices near the model surface. Figure 7 shows hot-film spectra for prerun, quiet, and noisy data that also suggest that the boundary layer is laminar toward the aft end of the model because the quiet-tunnel spectrum falls nearly on top of the prerun spectrum. The low power of the low frequencies, especially when compared with the noisy tunnel data, are indicative of a laminar boundary layer. A turbulent boundary layer is expected to have much higher power, especially for low frequencies.

The results for the noisy tunnel case are very different and clearly discernible in Figs. 5–7. For the noisy case, after the expected rise at the corner, the temperature rises at an increased rate starting at about $x = 17.8$ cm (7.0 in.), peaks at about $x = 26.8$ cm (10.6 in.), and then decreases to the end of the model. This sudden rise in surface temperature is a strong indicator of transition. The much higher power in the hot-film spectrum also strongly suggest transition under noisy tunnel conditions. From Fig. 6, it is reasonable to assume that centerline transition onset takes place at around $x = 14.0$ cm (5.5 in.). This is where the centerline surface temperature under noisy conditions significantly departs from that under quiet conditions.

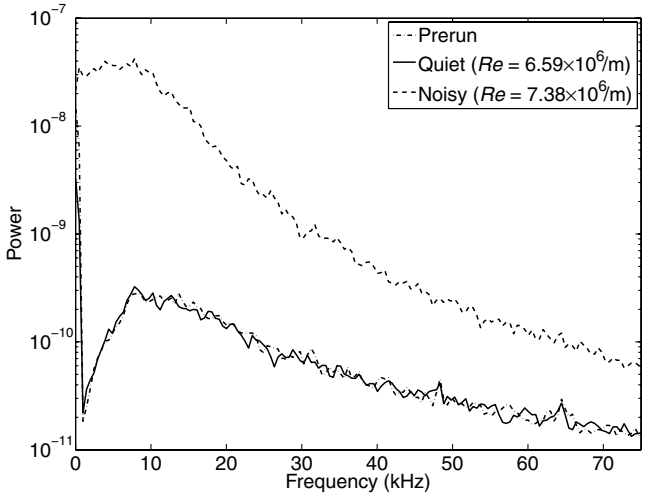

Fig. 7 Hot-film spectra for smooth insert for quiet and noisy flow.

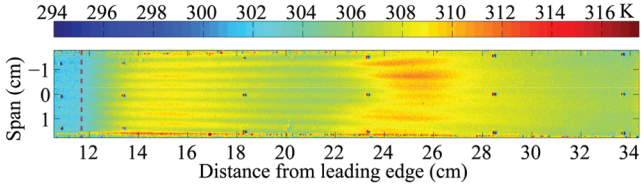

a) Surface temperature for quiet flow, ramp trips, Re=6.63x10⁶/m (2.02x10⁶/ft)

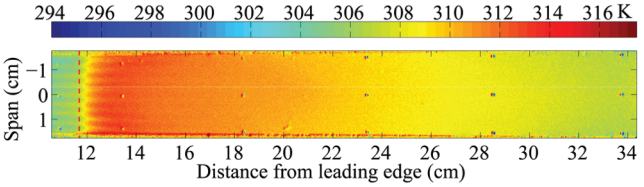

b) Surface temperature for noisy flow, ramp trips, Re=7.45x10⁶/m (2.27x10⁶/ft)

Fig. 8 Surface temperature (K) distribution with ramp trips under quiet and noisy conditions.

Although no hot-wire measurements were made to confirm these conclusions, hot-wire measurements with transition induced by roughness strips support these conclusions.

It is difficult to know whether the distance from the leading-edge, the distance from the strip, or the distance from the compression corner is the appropriate length parameter for transition. The presence of the compression corner almost certainly has a destabilizing effect on the boundary layer. However, it may be that the distance from the trips is the most important length factor. For the smooth-walled case, however, the distance from the nose is the most important length. Transition Reynolds numbers based on freestream conditions and all three lengths will be reported. It would be better to calculate the Reynolds number based on edge conditions, but at present this is not feasible.

Reducing freestream noise levels from conventional to quiet levels caused the transition Reynolds number, based on distance from the nose to transition onset, to increase by a factor of at least 2.2 from 1.03×10^6 to greater than 2.27×10^6. The actual increase cannot be determined because the flow is laminar past the end of the model under quiet conditions at the maximum quiet Reynolds number. The transition Reynolds number based on distance from the strip increases by a factor of at least 3.2 from 0.57×10^6 to at least 1.85×10^6. Based on distance from the corner, the transition Reynolds number increases by a factor of at least 8.9 from 0.17×10^6 to 1.50×10^6.

The vortices observed under quiet flow suggest that the dominant natural, untripped transition mechanism may not be the amplification and breakdown of first- or second-mode waves. Spanwise spreading of the streamwise vortices indicates outward-directed crossflow. Natural transition may be dominated by vorticity from the leading-edge or three-dimensional crossflow. Transition may also be due to some complex coupling of leading-edge vorticity, crossflow, and first- or second-mode waves with a shear layer instability above a separation bubble at the corner [1].

Ramp Roughness Insert

Figure 8 shows the surface temperature distribution with the ramp roughness strip under quiet and noisy conditions for $Re = 6.63$ and 7.45×10^6/m (2.02 and 2.27×10^6/ft), respectively. For the quiet case, $T_0 = 418$ K (752°R) and $P_0 = 586$ kPa (85 psia) whereas under noisy conditions $T_0 = 424$ K (763°R) and $P_0 = 627$ kPa (91 psia). There are clearly significant temperature changes in both the streamwise and spanwise directions. No single cut of temperature can completely capture these variations.

Figure 9 shows the streamwise centerline temperature as well as the streamwise temperature along the line $y = -0.2$ cm for both noisy and quiet cases. Here, each point along the centerline is the mean temperature of a 9-by-7-pixel rectangle, and each point along

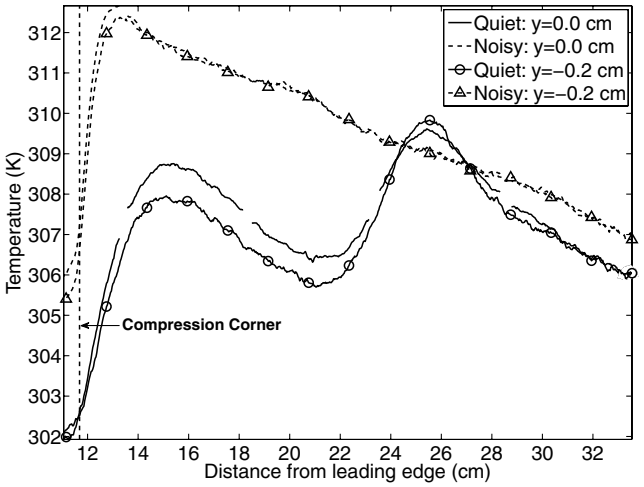

Fig. 9 Streamwise temperature for centerline and $y = -0.2$ cm (−0.08 in.) for ramp trips for quiet and noisy flow at $Re = 6.63$ and 7.45×10^6/m (2.02 and 2.27×10^6/ft).

$y = -0.2$ cm (−0.0 8 in.) is the mean temperature of a 9-by-3-pixel rectangle. The size of the averaging rectangles were different because of the large temperature gradients in the y direction and the relatively thin regions of lower temperature between the high-temperature streamwise streaks. Figure 10 shows several spanwise temperature distributions under quiet flow. Figure 11 shows spectra of the surface hot-film signal.

The significant difference between quiet and noisy flow is immediately evident from the images. Along the centerline for the quiet case, the temperature increases by about 6 K (11°R) from the compression corner to $x = 15.2$ cm (6 in.). This is significantly higher heating than for the smooth-insert case shown in Fig. 6, which increased by only about 1 K (2°R) downstream of the corner. This region of high heating is followed by a decrease in temperature from $x = 15.5$ cm (6.1 in.) to $x = 21.6$ cm (8.5 in.). At this point, the temperature increases sharply to a second peak at $x = 25.7$ cm (10.1 in.) followed by a gradual decrease to the end of the model.

It seems likely that the first temperature rise is due to the combination of compression heating as well as heating due to the laminar vortices near the model surface that are shed from the trip elements. The streamwise streaks in Fig. 8a are most likely due to these vortices. In Fig. 9, the centerline streamwise temperature is along a peak in spanwise temperature of Fig. 10. The streamwise temperature along $x = -0.2$ cm is along a trough in the spanwise distribution. The maximum difference between peak and trough

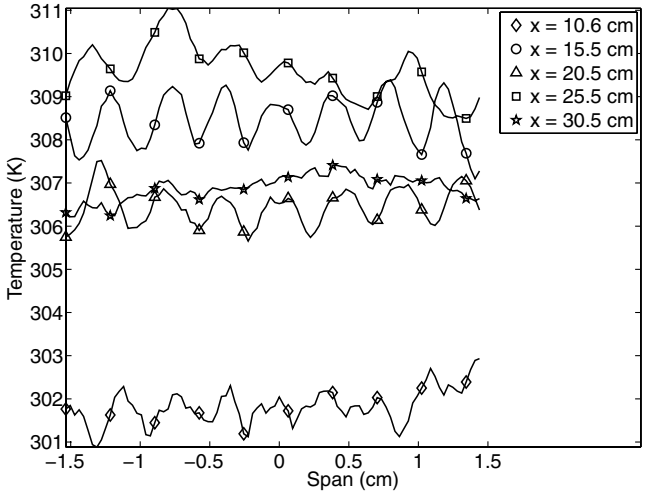

Fig. 10 Spanwise temperature at several streamwise locations for quiet flow at $Re = 6.63 \times 10^6/\text{m}$ ($2.02 \times 10^6/\text{ft}$).

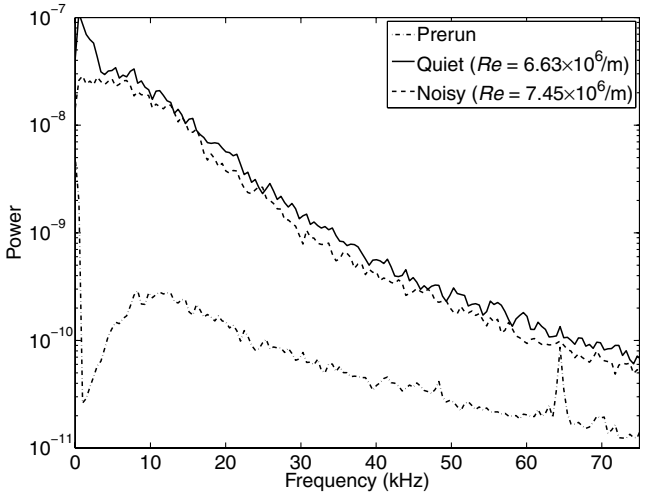

Fig. 11 Hot-film spectra for quiet and noisy flow with ramp trips.

temperatures is only about 1 K (2°R) under quiet conditions with almost no difference under conventional freestream noise levels.

The streamwise temperature decrease after the first peak is attributed to the thickening laminar boundary layer. The second temperature increase, starting at around $x = 21.6$ cm (8.5 in.), is thought to be due to the onset of transition. Schneider [1] states that the maximum surface temperature generally corresponds to the middle of transition. Thus, at $x = 26.7$ cm (10.5 in.), it seems that the boundary layer is well on its way to being fully turbulent with the subsequent temperature decrease due to the thickening turbulent boundary layer.

Under conventional noise levels, this type of behavior is not seen. Rather, there is a sharp rise in temperature from the corner $x = 11.7$ cm (4.6 in.) to $x = 14.0$ cm (5.5 in.). This high-temperature peak is then followed by a nearly monotonic decrease to the end of the model. The sudden rise in surface temperature and subsequent decrease suggests that the boundary layer transitions just downstream of the corner. The hot-film spectra in Fig. 11 support the contention that the windward boundary layer has transitioned at the hot film ($x = 26.7$ cm, 10.5 in.) under both quiet and noisy flow. The spectra lie almost on top of each other and show high power levels at the lower frequencies.

The spanwise temperatures at streamwise stations of $x = 10.6$, 15.5, 20.5, 25.5, and 30.5 cm (4.1, 6.1, 8.1, 10.0, and 12.0 in.) in Fig. 10 clearly reflect the temperature behavior shown in Fig. 9. The oscillations seen at $x = 15.5$, 20.5, and 25.5 cm (6.1, 8.1, and

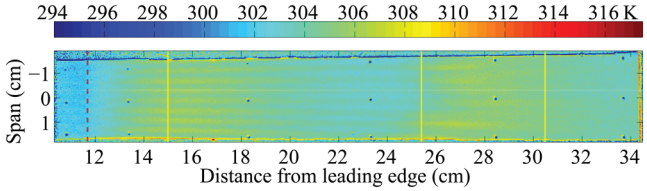

Fig. 12 Surface temperature for quiet flow with ramp trips at $Re = 5.87 \times 10^6/\text{m}$ ($1.79 \times 10^6/\text{ft}$).

10.0 in.) are no longer visible by $x = 30.5$ cm (12.0 in.). Over most of the ramp, there is little axial growth of the oscillations. Rather, they seem to saturate and then break down. This is further indication of a turbulent boundary layer on the aft portion of the model.

Figure 12 shows the windward temperature distribution at $Re = 5.87 \times 10^6/\text{m}$ ($1.79 \times 10^6/\text{ft}$) for the ramp roughness trip at the reduced maximum quiet pressure used for the hot-wire measurements. Figure 13 shows the centerline temperature. Here, $T_0 = 427$ K (769°R) and $P_0 = 538$ kPa (78 psia). In Figs. 12 and 13, the solid lines mark the streamwise locations of the hot-wire measurements. The dashed lines show the corner location. Qualitatively, the temperature behaves very similarly to what was seen in Figs. 8a and 9. There is an initial temperature rise downstream of the corner followed by a decrease, a sharp rise, and then a steady decrease to the end of the model. Because of the qualitative similarities, it was decided to proceed with the hot-wire measurements to determine the state of the boundary layer. The results were then extrapolated to the TSP images at the slightly higher Reynolds numbers used earlier.

To accurately determine the state of the boundary layer, runs with the hot wire positioned at $x = 15.0$, 25.4, and 30.5 cm (5.9, 10.0, and 12.0 in.) were first made with the hot wire traversing through the boundary layer in order to determine its thickness. The same hot wire was used for all three runs. Its typical square-wave frequency response was about 240 kHz. The overheat ratio based on resistances was about 1.8, making it most sensitive to mass flux. It was a Platinum/10% Rhodium wire with a diameter of 0.00038 cm (0.00015 in.) and a length/diameter ratio of about 107. The hot wire was always used with the 1:1 bridge of a TSI IFA-100 constant temperature anemometer. The Tektronix DPO7054 oscilloscope operating in Hi-Res mode was used to sample all hot-wire data. The sampling frequency was always 2×10^6 samples per second.

Generally, the hot wire began the run at 0.7 or 0.9 mm (0.03 or 0.04 in.) from the model surface. Over the course of about 6 s, it moved away from the model in 0.1 mm (0.004 in.) increments, stopping at each location for 200 ms. The distance from the wall at each step was then plotted against the average CTA bridge voltage. From this plot in Fig. 14 the approximate boundary-layer thickness was deduced.

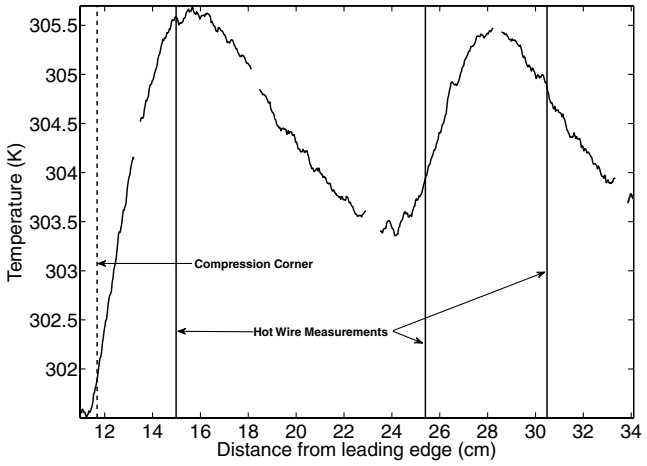

Fig. 13 Centerline temperature for quiet flow with ramp trips at $Re = 5.87 \times 10^6/\text{m}$ ($1.79 \times 10^6/\text{ft}$).

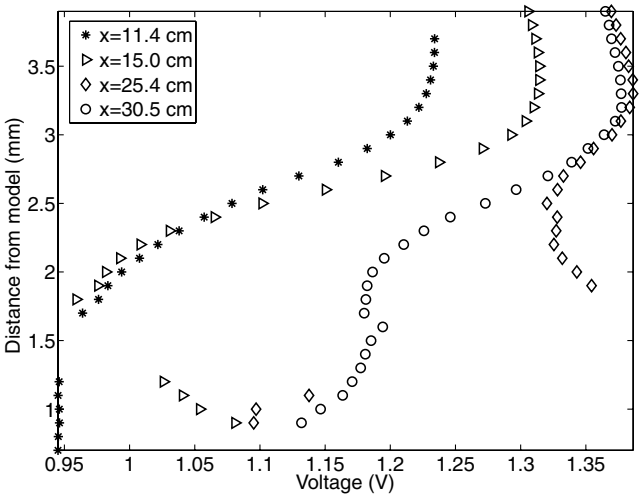

Fig. 14 Boundary-layer profiles.

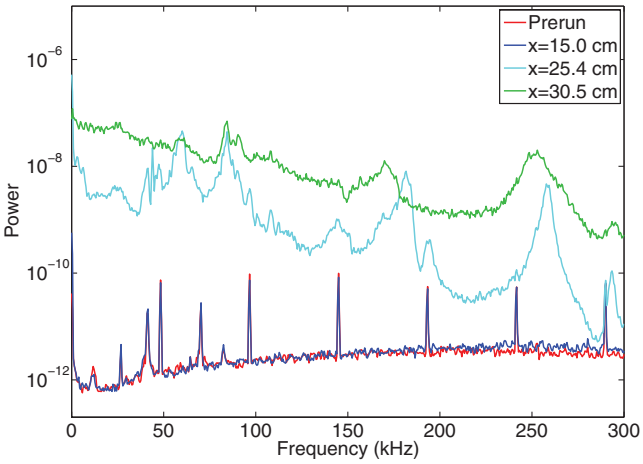

Fig. 15 Hot-wire spectra for ramp roughness at $Re \approx 5.9 \times 10^6$/m ($1.8 \times 10^6$/ft).

Over the course of a typical run, the Reynolds number dropped by about 35%. This means that by the end of the run, when the points furthest away from the model were recorded, the boundary layer was considerably thicker than at the beginning of the run. The hot-wire spectra were to be computed for data at around $t = 0.6$ s, where t is time from tunnel startup. The boundary-layer edge was not usually crossed until about $t = 4.5$ s. Thus, a scaling procedure was used to approximate the boundary-layer thickness at $t = 0.6$ s given a measured thickness at $t = 4.5$ s. This scaling assumes that transition did not move over the streamwise station of interest while the probe was traversing the boundary layer. It also assumes that the thickness is proportional to the inverse square root of the Reynolds number. The approximate boundary-layer thickness at $t = 0.6$ s can be determined from the thickness measured at $t = 4.5$ s through the following relation:

$$\frac{\delta(t=0.6)}{\delta(t=4.5)} \approx \sqrt{\frac{Re(t=4.5)}{Re(t=0.6)}} \approx \sqrt{\frac{P_0(t=4.5)}{P_0(t=0.6)}}$$

where δ is the boundary-layer thickness and P_0 is the stagnation pressure. The value of this ratio is generally around 0.85. A location about 15% less than the experimentally measured edge was usually chosen as the location to place the hot wire. This ensured that the hot wire was inside the boundary layer and near the edge at the time the spectra were computed. Also, it is expected and has been experimentally shown by Rufer and Schneider [18] in the BAM6QT that the amplitude of second-mode instability waves is greatest near the boundary-layer edge. Thus, if second-mode waves were present, it was thought that they would be visible in the hot-wire spectra.

Figure 14 shows the results of the boundary-layer profile runs for streamwise locations of $x = 11.4$, 15.0, 25.4, and 30.5 cm (4.5, 5.9, 10.0, and 12.0 in.). The gaps in the boundary-layer profiles are because of a lack of data due to nozzle-wall boundary-layer separation. Ideally, boundary-layer profiles would have been measured for these streamwise stations for both trip strips. However, due to probe difficulties, tunnel difficulties, and time constraints, profiles were measured for the ramp trips at only the three downstream locations and for the diamond trips for the $x = 11.4$ cm (4.5 in.) case. The boundary-layer thickness measured with the ramp trips was used as an approximate value for the diamond-roughness cases.

It is not a simple matter to obtain a value for the boundary-layer edge location. As can be seen, the voltage gradually approaches a peak value and then generally decreases again. An approximate value for the edge location is all that could be readily obtained. Finding a more accurate value for the boundary-layer edge at a specific time was beyond the scope of the current investigation.

Figure 15 shows the power spectra at $Re \approx 5.9 \times 10^6$/m ($1.8 \times 10^6$/ft) for streamwise hot-wire locations of $x = 15.0$, 25.4, and 30.5 cm (5.9, 10.0, and 12.0 in.) as well as spectra computed for the $x = 25.4$ cm (10.0 in.) prerun signal. The corresponding distances above the model surface were 2.7, 3.0, and 3.0 mm (0.11, 0.12, and 0.12 in.), respectively. The spectra were computed over a 200 ms interval. As much as was possible, they were computed over a portion of the signal for which the nozzle-wall boundary layer had no turbulent bursts. Each spectrum was the average of 100 fast Fourier transforms (FFTs), with each FFT computed from 4000 data points. Welch's averaged, modified periodogram method with a Hamming window was used.

As can be seen in Fig. 15, when the hot wire was located very near the first local peak in the centerline temperature, the spectrum at $x = 15.0$ cm (5.9 in.) falls nearly on top of the prerun spectrum. This indicates that there are very few disturbances in the boundary layer at that location and that it is laminar, as was previously suspected from the TSP data. The spectrum for $x = 25.4$ cm (10.0 in.) is very different from that at $x = 15.0$ cm (5.9 in.). The location $x = 25.4$ cm (10.0 in.) is just downstream of where the centerline temperature began to increase for the second time. It was suspected that this location was near to the midpoint of transition. The spectrum supports this notion. The power levels, especially for the lower frequencies, are orders of magnitude higher than the prerun and $x = 15.0$ cm (5.9 in.) spectra. It appears that the boundary layer at $x = 25.4$ cm (10.0 in.) may not be completely turbulent, but there are significant disturbances present at that location. The spectrum at $x = 30.5$ cm (12.0 in.), where it was suspected that the boundary layer had become fully turbulent, shows power levels generally at least a factor of 2 greater than for the $x = 25.4$ cm (10.0 in.) case. These high levels of broadband noise are due to a turbulent boundary layer at $x = 30.5$ cm (12.0 in.).

Because the hot wire and TSP data agree about the state of the boundary layer at the reduced quiet pressure, conclusions can be drawn from the TSP images at higher pressure even though there are no supporting hot-wire measurements. From Fig. 9, transition onset is taken to be at about $x = 21.0$ cm (8.25 in.) under quiet conditions at $P_0 = 586$ kPa (85 psia). It happens immediately downstream of the compression corner under noisy conditions. Reducing freestream noise levels from conventional to quiet levels caused the transition Reynolds number based on distance from the nose to increase by a factor of 1.6 from 0.87×10^6 to 1.39×10^6. The transition Reynolds number based on distance from the strip increases by a factor of 2.4 from 0.40×10^6 to 0.97×10^6. Based on distance from the corner, the transition Reynolds number increases from 0 to 0.68×10^6. Under the reduced quiet pressure conditions, transition was taken to be at $x = 24.1$ cm (9.5 in.). For the three different length parameters, this gave transition Reynolds numbers 1.42, 1.05, and 0.79×10^6, respectively.

This large effect of freestream noise levels on transition is not altogether surprising. The wake behind large roughness elements is often unstable. When freestream noise levels are elevated, increased

disturbance levels can be introduced into the unstable wake via a receptivity process. The growth of wake instabilities, thus, starts at a higher level, which can then lead to earlier breakdown and transition of the boundary layer [19].

Diamond Roughness Insert

A similar set of experiments was carried out with the diamond trips in the model. Figure 16 shows the surface temperature distribution with the diamond roughness strip under quiet and noisy conditions for 6.73 and 7.35×10^6/m (2.05 and 2.24×10^6/ft), respectively. For the quiet case, $T_0 = 422$ K (760°R) and $P_0 = 607$ kPa (88 psia). For the noisy case, $T_0 = 424$ K (763°R) and $P_0 = 614$ kPa (89 psia). Figure 17 shows the streamwise centerline temperature for both cases as well as the streamwise temperature along $y = -0.4$ cm (-0.16 in.), a trough in the spanwise temperature. Figure 18 shows spanwise temperatures at several streamwise stations under quiet flow. Figure 19 shows the spectra of the surface hot-film signal.

As the figures show, qualitatively, the surface temperature behaves very similarly to the ramp-roughness case. Under quiet conditions, just downstream of the compression corner, there is an initial temperature rise. This is followed by a decrease, another sharp rise, and then a gradual reduction of the surface temperature. Additionally, high-temperature streaks are visible from upstream of the corner to the second temperature rise. The locations of the temperature peaks are upstream of the ramp-roughness case, however, occurring at $x = 13.7$ and 21.3 cm (5.4 and 8.4 in.) instead of $x = 15.5$ and 25.7 cm (6.1 and 10.1 in.), respectively.

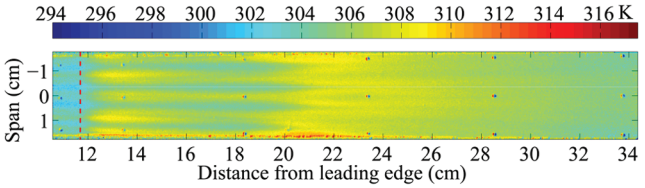

a) Surface temperature for diamond trips, quiet flow, Re=6.73 x 10⁶/m (2.05 x 10⁶/ft)

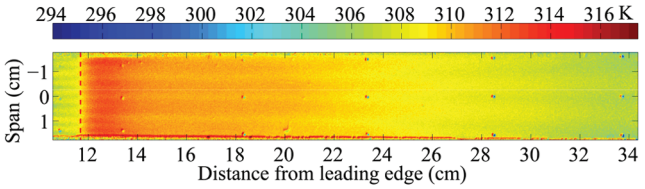

b) Surface temperature for diamond trips, noisy flow, Re=7.35 x 10⁶/m (2.24 x 10⁶/ft)

Fig. 16 Surface temperature (K) with diamond trips under quiet and noisy conditions.

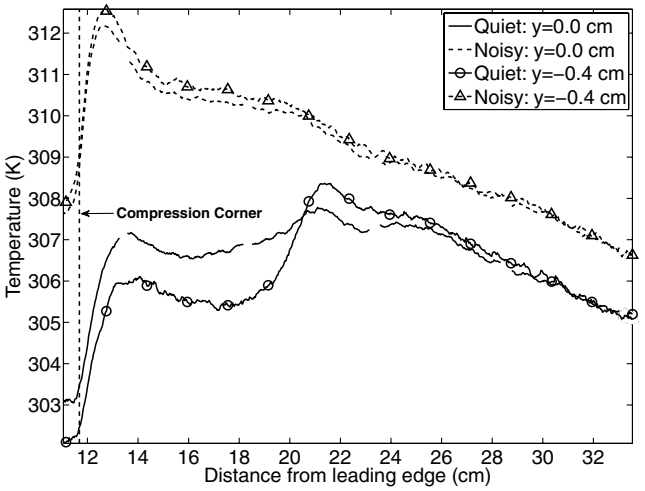

Fig. 17 Streamwise temperature for centerline and $y = -0.4$ cm (-0.16 in.) for diamond trips, quiet and noisy flow, at $Re = 6.73$ and 7.35 x 10⁶/m (2.05 and 2.27 x 10⁶/ft).

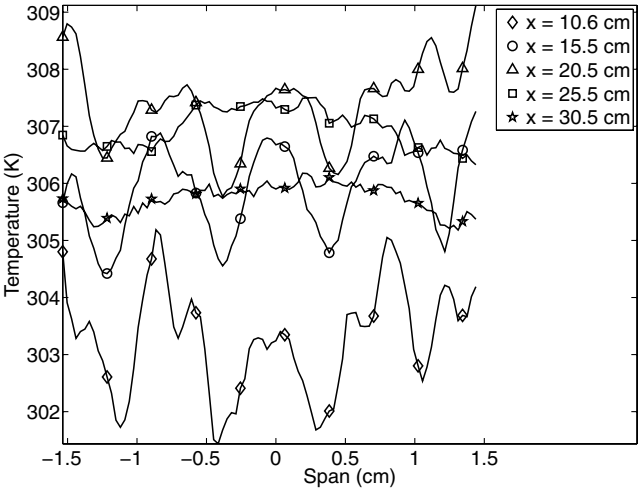

Fig. 18 Spanwise temperature at various streamwise locations for quiet flow with diamond trips.

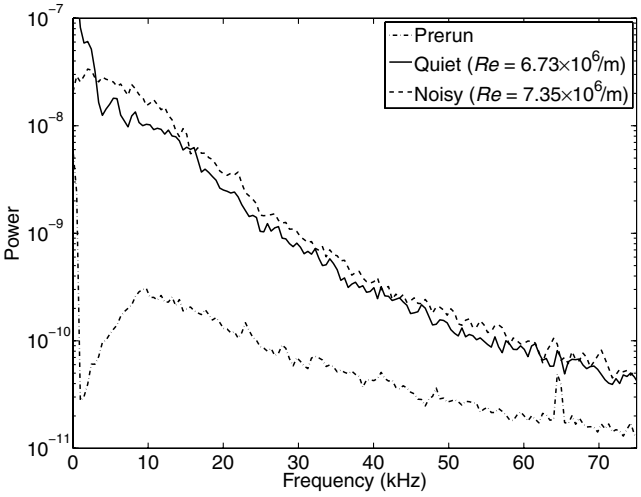

Fig. 19 Spectra for noisy and quiet flow with diamond trips.

The spanwise temperatures at streamwise stations of $x = 10.6$, 15.5, 20.5, 25.5, and 30.5 cm (4.1, 6.1, 8.1, 10.0, and 12.0 in.) in Fig. 18 clearly reflect the temperature behavior shown in Figs. 16a and 17. The mean temperature of the spanwise plots increases and decreases in a similar fashion to what is seen along the model centerline. Additionally, the spanwise oscillations are easily discernible for streamwise locations of $x = 10.6$, 15.5, and 20.5 cm (4.1, 6.1, and 8.1 in.). At $x = 25.5$ and 30.5 cm (10.0 and 12.0 in.), the oscillations are gone and the curve is much more smooth. This behavior is present in Fig. 16a as the streamwise streaks fade toward the aft end of the model.

Because of the qualitative similarities to the ramp-roughness case, it was thought that the first temperature rise was again due to compression heating at the corner and the presence of laminar vortices near the model surface. The second peak was again believed to be due to transition. The hot-film spectra support this theory for the runs at 0.655 MPa (95 psia) initial stagnation pressure, showing high power levels in the low-frequency band.

Again, due to the reduced maximum quiet pressure for the later hot-wire experiments in the BAM6QT, a TSP image was again taken under reduced pressure conditions before checking the boundary-layer state with a hot wire. Here, $Re = 5.84 \times 10^6$/m (1.78×10^6/ft), $T_0 = 427$ K (769°R), and $P_0 = 0.538$ MPa (78 psia). The surface temperature distribution can be seen in

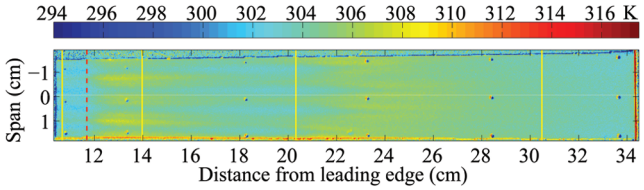

Fig. 20 Surface temperature for quiet flow with diamond trips at $Re = 5.84 \times 10^6$/m (1.78×10^6/ft).

Fig. 20. The centerline temperature is shown in Fig. 21. The dashed lines mark the compression corner and the solid lines are the locations at which spectra were computed. A brief comparison shows very similar behavior to that of Figs. 16a and 17, the surface and centerline temperature distributions for quiet flow at 0.655 MPa (95 psia). The locations of the temperature peaks are moved somewhat downstream from the similar peaks observed at $Re = 6.73 \times 10^6$/ m (2.05×10^6/ ft), but the qualitative similarities are sufficient reason to believe that the boundary layer behaves in the same way as for the higher-Reynolds-number case.

Figure 22 shows hot-wire spectra at $x = 10.7$, 14.0, 20.3, and 30.5 cm (4.2, 5.5, 8.0, and 12.0 in.) for distances from the surface of 3.0, 2.7, 2.8, and 3.0 mm (0.12, 0.11, 0.11, and 0.12 in.), respectively. The first hot-wire location $x = 10.7$ cm (4.2 in.) is 1.0 cm (0.4 in.) upstream of the compression corner. A power spectrum was also computed for 200 ms of prerun data for comparison.

It was at first surprising to find that the boundary layer was thicker at $x = 10.7$ cm (4.2 in.) than for locations further downstream.

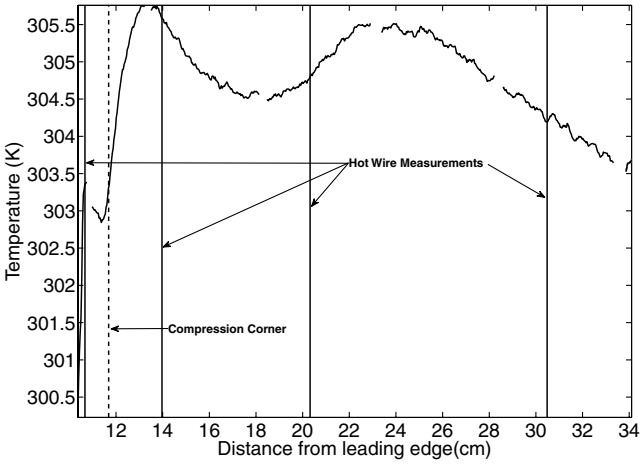

Fig. 21 Centerline temperature for quiet flow with diamond trips at $Re = 5.84 \times 10^6$/m (1.78×10^6/ft).

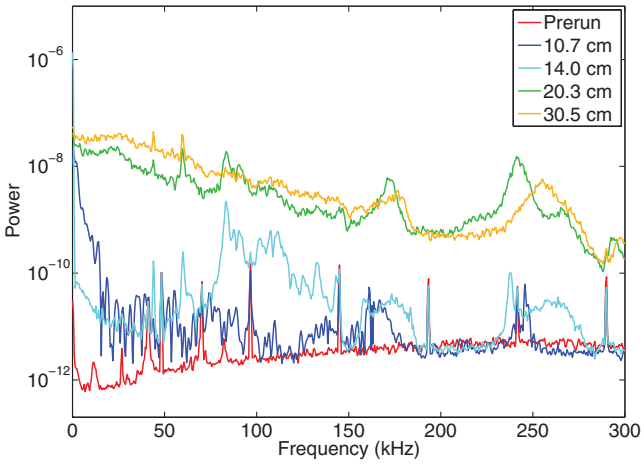

Fig. 22 Hot-wire spectra for diamond roughness.

Given the unique nature of the flow, however, this is not too difficult to explain. The flow at these locations is downstream of large roughness elements. In addition, it seems likely that there is a separation bubble at the compression corner. The effects and extent of such a separation, upstream and downstream, are not fully understood. Boundary-layer separations in hypersonic flow have been shown to extend up to 100 boundary-layer thicknesses upstream of the initial cause of the separation [20]. It may also be that downstream of the reattachment point it takes a considerable distance for the boundary layer to fully process the effects of the separation. Also, it is clear from the vortices in the TSP images that there is some outward-directed crossflow. This certainly affects the boundary-layer thickness.

These data again support what the TSP images suggest. Because of lower power levels at $x = 10.7$ and 14.0 cm (4.2 and 5.5 in.) compared with locations further downstream, it is concluded that the boundary layer is laminar at those locations. However, the power levels are higher and much less smooth than for the ramp roughness insert. The diamond roughnesses are 0.15 cm (0.060 in.) high, whereas the ramps have a maximum height of 0.076 cm (0.030 in.). The larger roughness gives rise to greater disturbances in the boundary layer, evidenced by higher and more uneven power levels in the power spectra. The trends in the spectra at $x = 20.3$ and 30.5 cm (8.0 and 12.0 in.) suggest a turbulent boundary layer. This is somewhat surprising for the $x = 20.3$ cm (8.0 in.) location. From Fig. 21, this location is just downstream of onset of the second temperature rise. It was thought that this second rise marked the onset of transition. As such, generally higher power levels were expected but not to the degree as those that were observed. It is possible that either the larger roughnesses and the resultant large disturbances cause the boundary layer to complete transition over a very short streamwise distance or that the boundary layer has not completely transitioned at $x = 20.3$ cm (8.0 in.). At $x = 20.3$ cm (8.0 in.), the power levels are lower than those at $x = 30.5$ cm (12.0 in.) for most frequencies, signifying that it may not yet be entirely turbulent.

Extrapolating trends back to the higher Reynolds number TSP results, transition onset is observed to occur in Fig. 17 at $x = 16.6$ cm (6.5 in.) under quiet conditions. Under noisy conditions, a fully turbulent boundary layer is seen just downstream of the corner. Reducing freestream noise levels from conventional to quiet levels caused the transition Reynolds number based on distance from the nose to increase by a factor of 1.3 from 0.86×10^6 to 1.11×10^6. The transition Reynolds number based on distance from the strip increases by a factor of 1.7 from 0.4×10^6 to 0.69×10^6. Based on distance from the corner, the transition Reynolds number increases from 0 to 0.39×10^6. Under the reduced quiet pressure conditions, transition was taken to be at $x = 18.3$ cm (7.2 in.). For the three different length parameters, this gave transition Reynolds numbers of 1.07, 0.70, and 0.45×10^6, respectively.

The increase in transition Reynolds number is not as substantial as that observed with the ramp trips. This result is not surprising, however, given the larger height of the diamond trips and the fact that both the ramp and diamond trips induced transition at the corner under noisy conditions. Thus the diamond roughness introduces much larger disturbances into the boundary layer and causes earlier transition under quiet conditions.

Growth of Streamwise Vortices in Quiet Flow

The streamwise vortices shed from upstream roughness elements are readily apparent in Figs. 8a and 16a. The rate at which they grow with increasing streamwise distance is of interest.

As shown in Fig. 23, the spanwise root-mean-square (rms) temperature can be a useful metric for determining the effect, growth, and breakdown of these streamwise vortices. Here, the rms for the row of spanwise pixels at each streamwise station was computed. The data were then smoothed by computing the average of the rms at a particular streamwise station with the rms values for the 4 adjacent pixels both upstream and downstream of the target station. Streamwise stations that included registration marks were not included. The gaps in data in Fig. 23 are due to the presence of

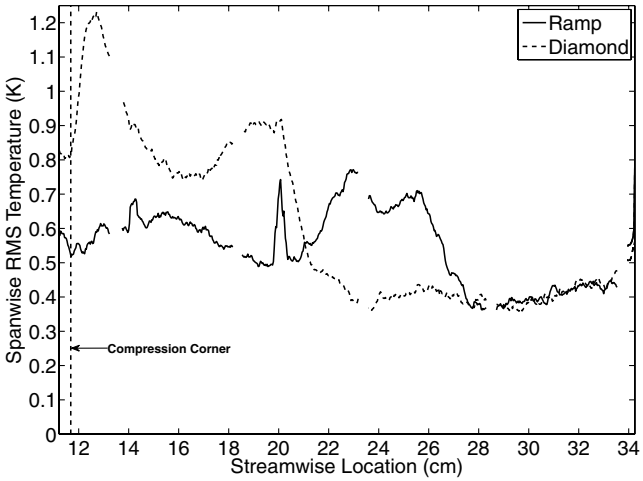

Fig. 23 Spanwise rms temperature as a function of streamwise distance for ramp and diamond trips.

registration marks at those stations. The vertical dashed line is again the location of the compression corner.

For both the ramp and diamond cases, the same qualitative pattern of spanwise rms is observed. There is an initial rise in the spanwise rms temperature immediately downstream of the compression corner. This is followed by a substantial decrease, a sharp rise, and then a sharp drop. This behavior can, perhaps, be best understood by the growth, decay, and breakdown of streamwise vortices in the flow. The incoming vortices are likely amplified by the compression corner, especially if there is a separated region there. The vortices then decay in the thickening laminar boundary layer for a few centimeters downstream of the corner. Then, from $x = 16$–20 cm (6.3–7.9 in.) for the diamond case and 20–25 cm (7.9–9.8 in.) for the ramp-roughness case, the vortices amplify significantly, increasing the rms temperature. The sharp drop in rms temperature is then likely due to breakdown of the vortices into a fully turbulent boundary layer. From $x = 28.0$ to 34.4 cm (11.0 to 13.5 in.), the spanwise rms temperature is nearly the same for both the ramp and diamond cases. This supports the idea that the streamwise vortices have broken down on the aft portion of the model for both cases.

The effect of the larger trip elements is immediately evident in Fig. 23. In the case of the diamond trips, the amplification at the corner seems to be significantly greater than with the ramp roughnesses, as evidenced by the much larger rms temperature there. The increase in rms temperature due to the amplification of the streamwise vortices begins at $x = 17$ cm (6.7 in.). This is about 4 cm (1.6 in.) upstream of the ramp case, where the rms begins increasing at about $x = 21$ cm (8.3 in.). The earlier amplification and breakdown of the streamwise vortices for the diamond trips seems to be due to the larger initial strength of the vortices shed from the higher diamond trips.

Conclusions

The effect of tunnel noise on natural and roughness-dominated transition was clearly seen on the 20%-scale X-51A forebody model in the BAM6QT. On the smooth model, no transition was observed in the TSP under quiet flow at $Re = 6.60 \times 10^6/\text{m}$ (2.01×10^6 ft), giving a transition Reynolds number based on distance from the leading edge of at least 2.27×10^6. When the tunnel was noisy, however, a clear transition front was seen by about $x = 17.8$ cm (7.0 in.) with an associated transition Reynolds number of 1.03×10^6. Reducing freestream noise from conventional to quiet levels increased the transition Reynolds number based on freestream conditions and length from the nose by a factor of at least 2.2.

With the ramp roughness strip in the model under quiet conditions at $Re = 5.87 \times 10^6/\text{m}$ ($1.79 \times 10^6/\text{ft}$), an initial temperature rise downstream of the compression corner was observed and attributed to laminar vortex heating. Further downstream, at about $x =$ 21.0 cm (8.3 in.), the onset of transition was observed with TSP and confirmed by hot-wire spectra. Under noisy conditions at $Re = 7.45 \times 10^6/\text{m}$ ($2.27 \times 10^6/\text{ft}$), the ramp roughnesses caused transition almost immediately downstream of the corner. Reducing freestream noise from conventional to quiet levels increased the transition Reynolds number by a factor of 2.4 where the length parameter is the distance from the strip.

The diamond roughness insert provided results qualitatively similar to those of the ramp roughness. Under quiet conditions at $Re = 5.87 \times 10^6/\text{m}$ ($1.78 \times 10^6/\text{ft}$), the location of peak laminar vortex heating as well as peak transitional heating was found to move upstream by around 5.1 cm (2.0 in.) when compared with the ramp-roughness results. Under noisy conditions at $Re = 7.35 \times 10^6/\text{m}$ ($2.24 \times 10^6/\text{ft}$), the boundary layer transitioned immediately downstream of the compression corner. Reducing freestream noise from conventional to quiet levels increased the transition Reynolds number by a factor of 1.7 where the length parameter is the distance from the strip.

It is well known that tunnel noise can have a profound effect on transition. In addition, a few previous experiments have shown an effect of tunnel noise on roughness-induced transition. However, to the author's knowledge, the present paper reports the first hypersonic measurements of roughness-induced transition under low noise levels that are comparable to flight, using reasonably sized trips.

If the trip size for the X-51A vehicle was based on results from wind tunnels with conventional noise levels, it is possible that the trips would be undersized. If so, transition on the vehicle would be delayed too far under the quiet conditions of flight. Clearly, quiet-tunnel results should be used to help determine the heights of such trips. However, it is not clear how to account for facility noise nor how to scale the trip sizes from facility to facility to flight. Further research is needed to develop methods of predicting the interaction and effect of freestream noise and roughness elements on transition.

Acknowledgments

This research is funded by AFOSR under grant FA9550-06-1-0182. Fabrication of the model was supported in part by The Boeing Company.

References

[1] Schneider, S. P., "Hypersonic Laminar-Turbulent Transition on Circular Cones and Scramjet Forebodies," *Progress in Aerospace Sciences*, Vol. 40, Nos. 1–2, 2004, pp. 1–50. doi:10.1016/j.paerosci.2003.11.001

[2] Beckwith, I. E., and Miller, C., III, "Aerothermodynamics and Transition in High-Speed Wind Tunnels at NASA Langley," *Annual Review of Fluid Mechanics*, Vol. 22, Jan. 1990, pp. 419–439. doi:10.1146/annurev.fl.22.010190.002223

[3] Schneider, S. P., "Effects of High-Speed Tunnel Noise on Laminar-Turbulent Transition," *Journal of Spacecraft and Rockets*, Vol. 38, No. 3, 2001, pp. 323–333. doi:10.2514/2.3705

[4] Schneider, S. P., "Flight Data for Boundary-Layer Transition at Hypersonic and Supersonic Speeds," *Journal of Spacecraft and Rockets*, Vol. 36, No. 1, 1999, pp. 8–20. doi:10.2514/2.3428

[5] Creel, T., Beckwith, I., and Chen, F., "Transition on Swept Leading Edges at Mach 3.5," *Journal of Aircraft*, Vol. 24, No. 10, Oct. 1987, pp. 710–717. doi:10.2514/3.45511

[6] Ito, T., Randall, L. A., and Schneider, S. P., "Effect of Noise on Roughness-Induced Boundary-Layer Transition for Scramjet Inlet," *Journal of Spacecraft and Rockets*, Vol. 38, No. 5, Sept. 2001, pp. 692–698. doi:10.2514/2.3754

[7] Wilkinson, S. P., Anders, S. G., and Chen, F.-J., "Status of Langley Quiet Flow Facility Developments," AIAA Paper 94-2498, June 1994.

[8] Beckwith, I., Creel, T., Chen, F., and Kendall, J., "Freestream Noise and Transition Measurements on a Cone in a Mach-3.5 Pilot Low-Disturbance Tunnel," NASA TP 2180, Sept. 1983.

[9] Blanchard, A. E., Lachowicz, J. T., and Wilkinson, S. P., "NASA Langley Mach 6 Quiet Wind-Tunnel Performance," *AIAA Journal*,

Vol. 35, No. 1, Jan. 1997, pp. 23–28.
doi:10.2514/2.82
[10] Schneider, S. P., "Development of Hypersonic Quiet Tunnels," *Journal of Spacecraft and Rockets*, Vol. 45, No. 4, 2008, pp. 641-664.
[11] Lafferty, J. F., and Norris, J. D., "Measurements of Fluctuating Pitot Pressure, Tunnel Noise in the AEDC Hypervelocity Wind Tunnel No. 9," AIAA Paper 2007-1678, Feb. 2007.
[12] Liu, T., and Sullivan, J., *Pressure and Temperature Sensitive Paints*, Springer–Verlag, New York, 2005.
[13] Matsumura, S., Schneider, S. P., and Berry, S. A., "Streamwise Vortex Instability and Transition on the Hyper-2000 Scramjet Forebody," *Journal of Spacecraft and Rockets*, Vol. 42, No. 1, 2005, pp. 78–89.
doi:10.2514/1.3959
[14] Matsumura, S., Schneider, S. P., and Berry, S. A., "Flow Visualization Measurement Techniques for High-Speed Transition Research in the Boeing/AFOSR Mach-6 Tunnel," AIAA Paper 2003-4583, July 2003.
[15] Berry, S. A., Auslender, A. H., Dilley, A. D., and Calleja, J. F., "Hypersonic Boundary-Layer Trip Development for Hyper-X," *Journal of Spacecraft and Rockets*, Vol. 38, No. 6, 2001, pp. 853–864.
doi:10.2514/2.3775
[16] Schmisseur, J., Young, J., and Schneider, S. P., "Measurements of Boundary-Layer Transition on the Flat Sidewall of a Rectangular Mach 4 Quiet-Flow Nozzle," AIAA Paper 96-0852, Jan. 1996.
[17] Schneider, S. P., Collicott, S. H., Schmisseur, J., Ladoon, D., Randall, L. A., Munro, S. E., and Salyer, T. R., "Laminar-Turbulent Transition Research in the Purdue Mach 4 Quiet-Flow Ludwieg Tube," AIAA Paper 96-2191, June 1996.
[18] Rufer, S., and Schneider, S. P., "Hot-Wire Measurements of Instability Waves at Mach 6," AIAA Paper 2006-3054, June 2006.
[19] Schneider, S. P., "Effects of Roughness on Hypersonic Boundary-Layer Transition," *Journal of Spacecraft and Rockets*, Vol. 45, No. 2, 2008, pp. 193-209.
[20] Skoch, C., Schneider, S. P., and Borg, M. P., "Disturbances from Shock/Boundary Layer Interactions Affecting Upstream Hypersonic Flow," AIAA Paper 2005-4897, June 2005.
[21] Hank, J. M., Murphy, J. S., and Mutzman, R. C., "The X-51A Scramjet Engine Flight Demonstration Program," AIAA Paper 2008-2540, April 2008.

R. Kimmel
Associate Editor